

Investigation of Hydrogen Permeability in Metallic Materials for Bipolar Plates with Noble Coatings for PEMFC/PEMWE Systems

Hee-Gun Shin², Jae-Ho Lee², Seung-Pill Jung², Hyun-Yeong Jung², Song Jun Ho¹,
Yeon Joo Hong¹, Ei Joon Shim¹, and Hye-Jin Kim^{1,†}

¹Department of Advanced Materials Engineering, Tech University of Korea (TU Korea), Siheung-si, Gyeonggi-do, 15073, Republic of Korea

²Research & Development Division, Hyundai-Steel Company, Dangjin-si, Chungcheongnam-do, 31719, Republic of Korea

(Received August 01, 2025; Revised August 21, 2025; Accepted August 22, 2025)

The growing demand for durable PEM systems (PEMFCs and PEMWEs) has emphasized the significance of corrosion resistance and hydrogen uptake characteristics in metallic bipolar plates. To mitigate degradation in corrosive environments, noble metal coatings such as platinum (Pt) and gold (Au) have been applied; however, their effects on hydrogen permeation are not well understood. This study evaluates the hydrogen permeation characteristics of STS470, STS316L, and a titanium alloy using the Devanathan–Stachurski electrochemical method, both in bare form and with noble metal coatings. Thin layers of Pt and Au were deposited via sputtering, and testing was performed in simulated acidic electrolyte environments relevant to PEM operation. The results revealed that STS470 had the highest hydrogen permeability, while the titanium alloy exhibited the lowest. Both Pt and Au coatings significantly reduced hydrogen permeation, with Pt demonstrating slightly better performance. Furthermore, these coatings improved corrosion resistance under harsh electrochemical conditions. These findings highlight the dual role of noble metal coatings in reducing hydrogen uptake and enhancing corrosion resistance, providing valuable insights for designing advanced metallic bipolar plates in next-generation PEM systems.

Keywords: Hydrogen permeation, Bipolar plate, Stainless steel, Titanium alloy, Noble metal coatings

1. Introduction

Proton exchange membrane fuel cells (PEMFCs) have garnered significant attention due to their high energy efficiency, low operating temperature, and environmental compatibility, making them ideal for both automotive and stationary power generation applications. Among the core components of PEMFCs, metallic bipolar plates play a pivotal role in ensuring efficient current collection, gas separation, and structural support. In addition, they need as critical barriers against hydrogen permeation and corrosion, particularly under harsh electrochemical environments characterized by acidity and humidity.

Beyond PEMFCs, metallic bipolar plates are also essential components in proton exchange membrane water electrolyzers (PEMWEs). In PEMWE systems, the

operating conditions are even more severe, involving higher anodic potentials and elevated partial pressures of oxygen and hydrogen. The highly acidic and oxidizing electrolyte on the anode side requires materials with exceptional corrosion resistance and minimal hydrogen permeability. Therefore, the development of bipolar plate materials that can withstand both PEMFC and PEMWE environments is essential for the deployment of integrated hydrogen energy technologies.

Traditionally, graphite has been widely used as a bipolar plate material due to its excellent corrosion resistance and electrical conductivity. However, its brittleness, high manufacturing cost, and limited mechanical strength have driven the transition toward metallic alternatives [1]. Ferritic stainless steels (e.g., STS470), austenitic stainless steels (e.g., STS316L), and titanium alloys have emerged as promising candidates owing to their favorable mechanical properties and formability [2,3]. Nevertheless, these metallic materials still face challenges such as surface passivation—leading to increased interfacial contact resistance—and susceptibility to hydrogen

[†]Corresponding author: khj020911@tukorea.ac.kr

Hee-Gun Shin: Junior researcher, Jae-Ho Lee: Senior researcher, Seung-Pill Jung: Senior researcher, Hyun-Yeong Jung: Senior researcher, Song Jun Ho: Undergraduate student, Yeon Joo Hong: Undergraduate student, Ei Joon Shim: Undergraduate student, Hye-Jin Kim: Professor

ingress, which can result in hydrogen embrittlement, fuel loss, and long-term degradation [4,5].

To address these issues, surface modification strategies using noble metal coatings have been extensively explored. Thin films of platinum (Pt) and gold (Au) are particularly attractive because they not only improve corrosion resistance and surface conductivity but may also act as effective barriers against hydrogen diffusion [6,7]. However, comprehensive evaluations of hydrogen permeability in noble-metal-coated metallic bipolar plates—particularly under PEMFC- and PEMWE-like conditions—remain limited. In particular, the quantitative relationship between hydrogen transport behavior and microstructural characteristics has not been thoroughly investigated [8].

In this study, the hydrogen permeation behavior of three candidate metallic bipolar plate materials—STS470, STS316L, and a titanium alloy—was evaluated using the Devanathan–Stachurski electrochemical method. Both bare and sputter-deposited noble-metal-coated specimens (Pt and Au) were tested under simulated acidic conditions representative of PEMFC environments. The primary aim is to quantitatively assess the hydrogen barrier performance of noble metal coatings and to provide insight into optimal combinations of base metal and surface coating for long-term bipolar plate durability.

This research contributes to the advancement of high-

performance bipolar plates by offering a comparative understanding of hydrogen permeation behavior and the functional benefits of noble metal coatings in PEM systems⁹. The findings are expected to support future material selection strategies by correlating hydrogen resistance and electrochemical stability for both PEMFC and PEMWE applications.

2. Experiment

2.1 Materials

In both PEMFC and PEMWE systems, metallic bipolar plates serve as critical components that support electrical conduction, gas or water management, and mechanical integrity (Fig. 1). These plates are sandwiched between membrane electrode assemblies and are required to operate under highly aggressive electrochemical environments.

In PEMFCs, hydrogen is oxidized at the anode, and protons are transported through the membrane to the cathode, where oxygen reduction occurs. Although the operating voltage per cell is relatively low (~0.6–0.8 V), the bipolar plates must maintain corrosion resistance due to the consistently humid and mildly acidic environment.

In contrast, PEMWEs operate under reverse bias, where water is electrolyzed at the anode to produce oxygen and protons, while hydrogen is generated at the cathode. These systems typically require higher voltages (up to 2 V per

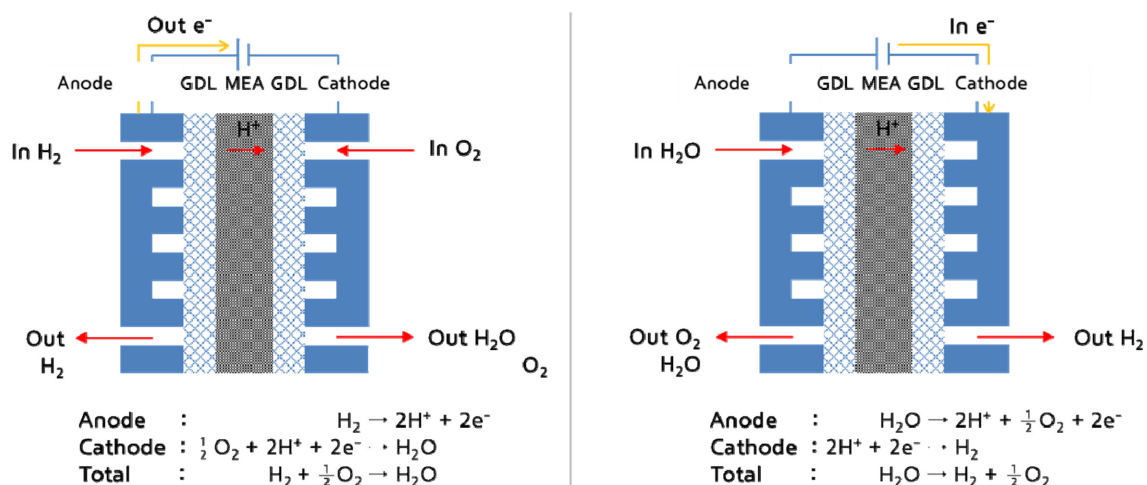


Fig. 1. Schematic representation of bipolar plate roles in (left) PEMFC and (right) PEMWE systems. Bipolar plates must withstand either anodic or cathodic conditions depending on their location, requiring high corrosion resistance and hydrogen impermeability

cell) and encounter more corrosive conditions due to intense oxygen evolution reactions in acidic electrolytes. As a result, bipolar plates in PEMWEs are subjected to stronger electrochemical driving forces and more aggressive degradation environments compared to those in PEMFCs.

Therefore, materials for bipolar plates in both systems must exhibit excellent corrosion resistance, low interfacial contact resistance, and minimized hydrogen permeability to ensure long-term durability and performance.

To meet these demanding requirements, this study investigates the hydrogen permeation and corrosion behavior of three candidate materials—ferritic stainless steel (STS470), austenitic stainless steel (STS316L), and a titanium alloy—each evaluated with and without noble metal coatings (Pt and Au). Thin 0.1 mm metallic foils were employed to simulate the actual thickness and geometry of bipolar plates. The noble metal coatings are expected to improve surface conductivity and serve as hydrogen diffusion barriers. Comparative electrochemical hydrogen permeation tests and post-test surface evaluations were conducted under simulated PEMFC-relevant conditions to quantify the performance of each material and coating combination.

To enhance corrosion resistance and suppress hydrogen permeation, platinum (Pt) and gold (Au) coatings were applied to one side of the metallic specimens via electrochemical deposition. The deposition processes for both metals were conducted under galvanostatic conditions in appropriately formulated aqueous baths. For Pt deposition, the electrolyte consisted of 5 g/L chloroplatinic acid hexahydrate ($\text{H}_2\text{PtCl}_6 \cdot 6\text{H}_2\text{O}$) dissolved in 50 g/L hydrochloric acid. The bath pH was maintained below 1 to ensure ionic conductivity and stability of Pt ions. The electrodeposition was carried out at a temperature of 60 °C with a constant current density of 1.0–1.5 mA/cm². A Pt mesh was used as the counter electrode, and the deposition time was adjusted between 10 to 20 minutes to achieve a coating thickness of approximately 100–150 nm. Magnetic stirring at 100–200 rpm was applied to maintain uniform ion distribution in the bath. For Au deposition, an alkaline sulfite-based electrolyte was used, consisting of 10 g/L sodium gold sulfite ($\text{Na}_3\text{Au}(\text{SO}_3)_2$) and 100 g/L sodium sulfite (Na_2SO_3). The pH of the bath was maintained in the range of 8–9. The plating process was conducted at a temperature of 50–60 °C under a

constant current density of 0.5–1.0 mA/cm². A Pt or Au mesh was used as the anode, and the plating time was set to 15–25 minutes to achieve a similar thickness to the Pt coating. Gentle stirring was applied during Au deposition to avoid excessive surface roughness.

After plating, all specimens were thoroughly rinsed with deionized water and dried with ethanol. The coated surfaces were visually inspected and then immediately subjected to hydrogen permeation testing to prevent surface contamination or oxidation.

2.2 Hydrogen permeability

Hydrogen permeation tests were conducted using a modified electrochemical technique based on ISO 17081. A Devanathan–Stachurski-type double-cell was employed to quantitatively evaluate hydrogen transport through metallic membranes under various surface coating and charging conditions [10]. The schematic of the experimental setup and specimen configuration is shown in Fig. 2 [10].

Test specimens—STS470, STS316L, and a titanium alloy—were fabricated into circular discs with a thickness of 0.1 mm and an exposed surface area of 1 cm² on each side. For selected samples, noble metal coatings (Pt and Au) were applied to one side of the specimen using an electrochemical (electroplating) method. The electroplating baths were prepared with suitable precursor solutions for Pt and Au deposition, and plating was performed under controlled current density and temperature conditions to ensure uniform and adherent films. After plating, the specimens were rinsed, dried, and immediately used for permeation testing.

On the detection side, a thin palladium (Pd) layer was used to catalyze the oxidation of permeated hydrogen, ensuring stable electrochemical response. The detection cell was filled with 0.1 M NaOH solution and continuously purged with nitrogen gas to prevent oxidative degradation. A constant anodic potential of +0.2 V vs. saturated calomel electrode (SCE) was applied in potentiostatic mode to facilitate the oxidation of hydrogen atoms diffusing through the membrane.

On the charging side, hydrogen absorption was initiated under galvanostatic conditions by applying a cathodic current density of -0.5 mA/cm² in a 3% NaCl + 0.3% NH_4SCN solution at room temperature. To simulate more

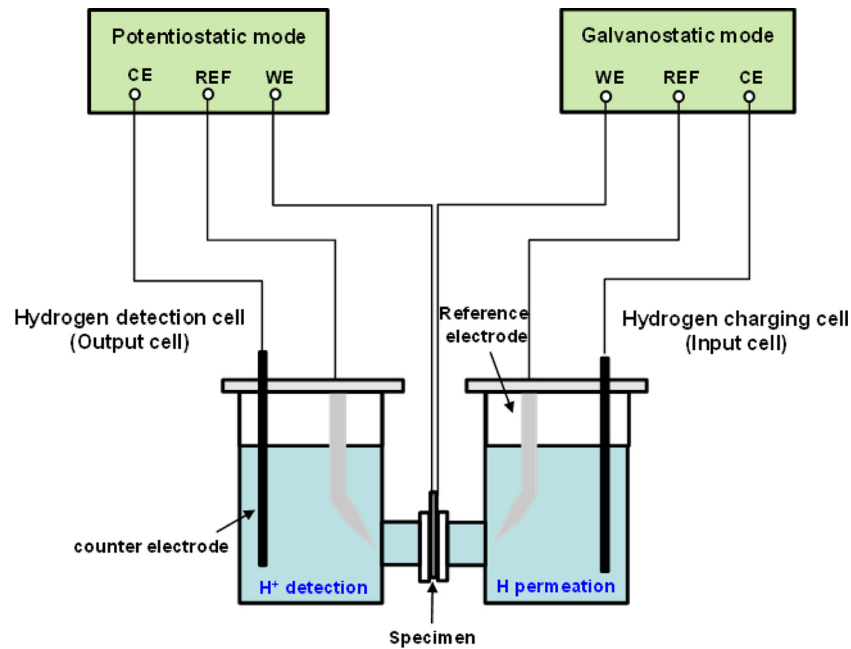


Fig. 2. Electrochemical hydrogen permeation double cell [10]

aggressive hydrogen flux scenarios, additional tests were conducted at elevated charging current densities of -50 and -500 mA/cm². These conditions enabled a more pronounced comparison of hydrogen permeability between bare and coated specimens.

The steady-state hydrogen permeation flux J_{ss} was calculated from the measured steady-state current I_{ss} , using the exposed electrode area (A) and the Faraday constant (F), according to equation (1):

$$J_{ss} = I_{ss}/AF \quad (1)$$

The effective diffusion coefficient (D_{eff}) was estimated from the lag time (t_{lag}) corresponding to 63% of the steady-state current using equation (2):

$$D_{eff} = L^2/6t_{lag} \quad (2)$$

The total hydrogen concentration at the entry surface (C_{0R}), including interstitial lattice and reversible trap sites, was calculated as using equation (3):

$$C_{0R} = J_{ss}L/D_{eff} \quad (3)$$

Assuming linear hydrogen concentration across the

specimen at steady-state using equation (4):

$$C(0,x) = C(1-x/L) \quad (4)$$

Lastly, the number of reversible hydrogen trap sites (N_t) was derived from the difference between lattice diffusivity (D) and effective diffusivity (D_{eff}) [$D = 7.28 \times 10^{-9} \text{ m}^2/\text{s}$] using equation (5):

$$N_t = C_{0R}/3 (D/D_{eff} - 1) \quad (5)$$

3. Results and Discussion

3.1 Hydrogen permeation behavior of candidate materials

The hydrogen permeation behavior of various metallic materials and coated specimens was investigated using the electrochemical Devanathan–Stachurski method. Fig. 3 illustrates the time-dependent permeation current density profiles for uncoated and noble metal-coated samples of STS470, STS316L, and Ti alloy, all with a uniform thickness of 0.1 mm.

First, this study establishes the baseline hydrogen permeation behavior of the uncoated materials. As shown in Fig. 3a, among the bare specimens, STS470 (labeled as 470FC, 0.1t) exhibited the highest hydrogen permeation

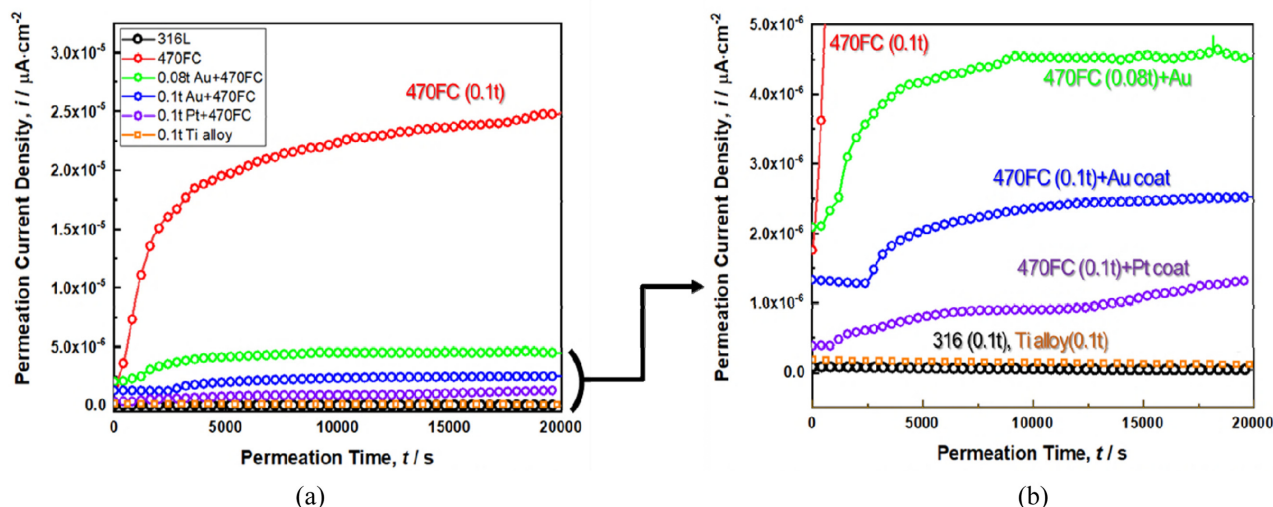


Fig. 3. Hydrogen permeation results: (a) permeation flux on various materials under $-0.5 \text{ mA}/\text{cm}^2$ condition and (b) enlarged regions in low flux level

current density, exceeding $2.5 \times 10^{-5} \mu\text{A}\cdot\text{cm}^{-2}$. This result is attributed to its ferritic body-centered cubic (BCC) crystal structure, which, although characterized by relatively low hydrogen solubility, enables fast and continuous hydrogen diffusion due to its high lattice diffusivity.

In contrast, as illustrated in Fig. 3b, both the austenitic STS316L and the HCP-structured Ti alloy showed negligible hydrogen permeation under identical test conditions. The Ti alloy's low hydrogen flux is ascribed to its densely packed hexagonal structure, which limits diffusion pathways, while STS316L exhibits strong hydrogen trapping behavior associated with its austenitic phase. These materials are known for their excellent hydrogen barrier properties and thus serve as reliable baseline references for comparative evaluation.

Second, the effectiveness of noble metal coatings on STS470 was examined to assess their potential for practical application. A substantial reduction in hydrogen permeation was observed after the application of Au and Pt coatings. In the case of Au, both 80 μm and 100 μm thick coatings markedly suppressed hydrogen diffusion. The 100 μm Au layer (0.1t) yielded better performance, indicating the importance of coating thickness and continuity in achieving an effective diffusion barrier. The steady-state permeation current was reduced to approximately $4 \times 10^{-6} \mu\text{A}\cdot\text{cm}^{-2}$, demonstrating successful surface passivation and hydrogen blocking, as shown in

Fig. 3b.

Pt-coated STS470 exhibited an even lower permeation current density ($\sim 1.2 \times 10^{-6} \mu\text{A}\cdot\text{cm}^{-2}$), outperforming the Au-coated counterpart ($\sim 2.5 \times 10^{-6} \mu\text{A}\cdot\text{cm}^{-2}$). This superior performance is attributed to Pt's enhanced electrochemical stability and the formation of a denser, more uniform electroplated layer, which likely minimizes defect-mediated hydrogen ingress. These findings confirm that noble metal coatings are highly effective in mitigating hydrogen permeation in ferritic stainless steels, functioning as both physical diffusion barriers and electrochemical stabilizers. Moreover, the coatings improve surface integrity and resistance to localized corrosion under acidic conditions.

Finally, the comparative analysis (expanded view in the right panel of Fig. 3) highlights the distinct permeation trends in the low-current regime. A clear ranking of hydrogen permeability is established as follows:

Bare STS470 > Au-coated STS470 (0.08t) > Au-coated STS470 (0.1t) > Pt-coated STS470 > STS316L \approx Ti alloy

This trend demonstrates the combined influence of substrate microstructure and coating quality on hydrogen barrier performance. The Ti alloy and 316L showed baseline resistance, while coated 470FC samples approached similar performance levels, validating coating as a viable engineering solution for low-cost ferritic

stainless steels. It further validates the use of noble metal-coated stainless steels as cost-effective and high-performance bipolar plate candidates for PEM systems.

3.2 Hydrogen Permeation Behavior of Candidate Materials

To quantitatively assess the hydrogen permeation resistance of bare and coated metallic materials, Devanathan–Stachurski electrochemical permeation tests were conducted under galvanostatic hydrogen charging (-0.5 mA/cm^2) in 3% NaCl + 0.3% NH_4SCN solution. The specimens included bare SUS 470FC, noble metal-coated variants (Au, Pt), SUS 316L, and a Ti alloy. Fig. 3 shows the steady-state permeation current densities as a function of time, confirming the clear retardation in hydrogen ingress upon surface modification.

As shown in Table 1. Electrochemical hydrogen permeation tests were conducted on STS470 (0.1t), both uncoated and coated with noble metals, to evaluate the effect of surface modification on hydrogen transport properties. The quantitative parameters—including effective diffusivity (D_{eff}), steady-state permeability (J_{ss}), hydrogen concentration at the entry side (C_{0R}), and trap density (N_T)—were calculated based on ISO 17081:2014 methodology.

The effective hydrogen diffusivity (D_{eff}), hydrogen permeation flux (J_{ss}), hydrogen concentration at the entry surface (C_{0R}), and density of reversible hydrogen trap sites (N_T) were calculated from the permeation profiles and are summarized in Table X. The results highlight the following trends. Bare SUS 470FC exhibited the highest J_{ss} value ($2.59 \times 10^{-6} \text{ mol/m}^2\cdot\text{s}$) and effective diffusivity ($1.505 \times 10^{-12} \text{ m}^2/\text{s}$), reflecting its relatively low resistance to hydrogen ingress. The Au-coated 470FC (0.1t Au and 0.08t Au) showed a substantial reduction in both J_{ss}

(2.90×10^{-7} and $4.17 \times 10^{-7} \text{ mol/m}^2\cdot\text{s}$, respectively) and D_{eff} ($\sim 8.5 - 9.5 \times 10^{-13} \text{ m}^2/\text{s}$), suggesting that Au coatings effectively mitigate hydrogen uptake by forming a barrier to hydrogen diffusion. Finally, Pt-coated 470FC (0.1t Pt) exhibited the lowest permeability among the coated samples ($J_{\text{ss}} = 1.87 \times 10^{-7} \text{ mol/m}^2\cdot\text{s}$), with $D_{\text{eff}} = 3.506 \times 10^{-13} \text{ m}^2/\text{s}$. This indicates that Pt forms a more compact and inert barrier layer compared to Au. Furthermore, based on the difference between lattice diffusivity ($7.28 \times 10^{-9} \text{ m}^2/\text{s}$) and D_{eff} , the density of hydrogen trap sites (N_T) was estimated. Bare 470FC exhibited the highest trap site density ($1.19 \times 10^{-6} \text{ mol/m}^3$), while noble metal-coated samples showed lower values (in the range of $1.33 - 8.54 \times 10^{-8} \text{ mol/m}^3$), indicating a reduction in the number of reversible trapping sites due to surface passivation effects.

In contrast, SUS 316L and Ti alloy showed negligible steady-state current within the testing period, suggesting that hydrogen permeation was below the detection limit under the given charging conditions. This confirms their inherently high hydrogen permeation resistance, likely due to the stable passive oxide layers. The Ti alloy and SUS 316L demonstrated negligible hydrogen permeation under standard conditions, reinforcing their suitability for hydrogen-related applications.

These findings reinforce that surface coatings, especially with electrochemically deposited Pt, significantly enhance the hydrogen barrier properties of ferritic stainless steel. The results confirm that, despite the good mechanical and fabrication advantages of STS470, noble metal coatings are essential to meet durability and hydrogen resistance requirements in PEMFC and PEMWE systems. While Ti and 316L stainless steel were also evaluated, the hydrogen permeation current was below detection limits under the

Table 1. Values of parameters calculated from the hydrogen permeation tests

Material	Diffusivity D_{eff} (m^2/s)	Permeability J_{ss} ($\text{mol/m}^2/\text{s}$)	Hydrogen Concentration C_{0R} (mol/m^3)	Density of Hydrogen Trap N_T (mol/m^3)
470FC (0.1t)	1.505E-12	2.59E-6	1.72E-2	1.19E-6
470FC+ Au (0.1t)	8.451E-13	2.90E-7	3.07E-3	1.33E-7
470FC+Au (0.08t)	9.456E-13	4.17E-7	3.94E-3	1.53E-7
470FC+0.1t Pt	3.506 E-13	1.87E-7	5.32E-3	8.54E-7
316L (0.1t)	N/A	N/A	N/A	N/A
Ti Alloy (0.1t)	N/A	N/A	N/A	N/A

current experimental setup, consistent with their known low diffusivity and high hydrogen trapping capacity at ambient temperatures.

3.2 Effect of aggressive charging conditions on ti alloy permeation

To evaluate the hydrogen barrier performance of Ti alloy under more aggressive conditions—such as those encountered in high-voltage PEMWE operation or transient fuel cell loads—an additional set of hydrogen permeation tests was conducted by varying the hydrogen charging current density from the baseline -0.5 mA/cm^2 to elevated levels of -50 and -500 mA/cm^2 (Fig. 4).

At the standard condition of -0.5 mA/cm^2 (left panel, Fig. 4a), all three specimens—bare Ti alloy, Au-coated Ti, and Pt-coated Ti—exhibited minimal hydrogen permeation. The permeation current density remained below $1.0 \times 10^{-7} \text{ } \mu\text{A}\cdot\text{cm}^{-2}$ throughout the test duration. This result highlights the inherently low hydrogen diffusivity and high trapping capacity of the HCP-structured Ti alloy, which masks the additional contribution of surface coatings under mild conditions. Therefore, differentiation between coating effects was not feasible at this low input.

In contrast, when the charging current was increased to -50 and -500 mA/cm^2 , a substantial increase in permeation current was observed, especially for the 500 mA/cm^2 case (right panel, Fig. 4b). The following trends were noted:

At -50 mA/cm^2 , the permeation current density

slightly increased, but the magnitude remained below $1.0 \times 10^{-7} \text{ } \mu\text{A}\cdot\text{cm}^{-2}$. The response was still relatively stable, with limited capacity to differentiate material performance.

At -500 mA/cm^2 , the bare Ti alloy exhibited a measurable and sustained hydrogen flux, reaching up to $5.85 \times 10^{-7} \text{ } \mu\text{A}\cdot\text{cm}^{-2}$. A distinct transient behavior was observed, where permeation current peaked around 5000–7000 seconds and then gradually decreased. This could be attributed to hydrogen saturation at near-surface trap sites and subsequent diffusion into the bulk.

These results clearly indicate that under high-flux hydrogen charging, Ti alloy is no longer impervious, and its transport behavior becomes sensitive to surface condition and material saturation effects. This condition enables reliable comparison between coating effects and allows for quantitative analysis of hydrogen barrier characteristics.

In PEMWE applications, where the anode experiences anodic potentials and high oxygen evolution, hydrogen ingress on the cathode side can still occur under cyclic loading or shutdown conditions. The elevated charging test at -500 mA/cm^2 mimics such transient hydrogen exposure scenarios. Thus, these findings suggest that even Ti alloys, which show excellent performance under steady PEMFC conditions, must be evaluated under aggressive PEMWE-like environments for long-term reliability.

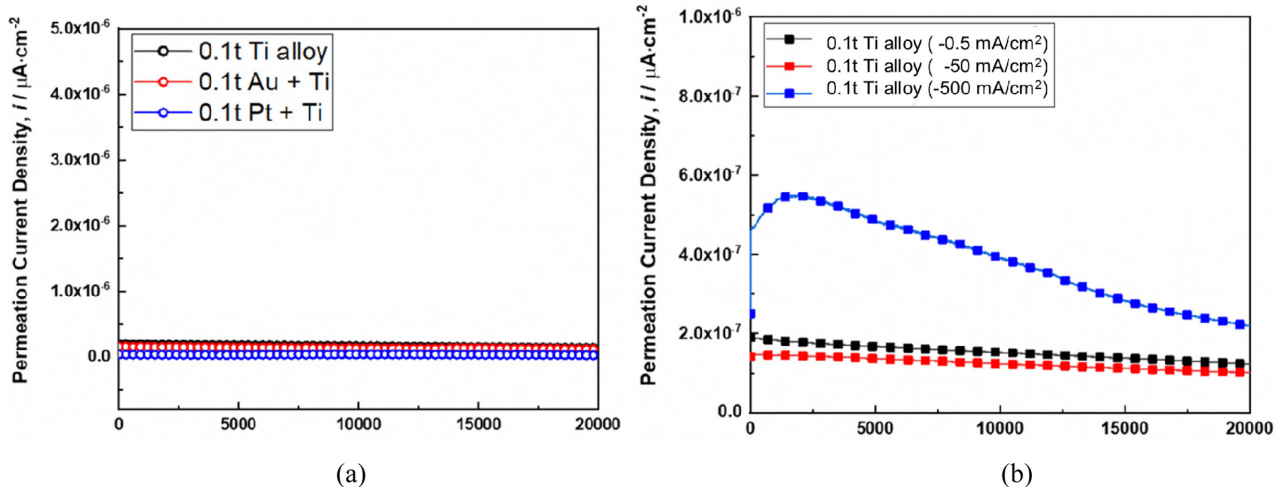


Fig. 4. Hydrogen permeation results: (a) -0.5 mA/cm^2 charging case on coating conditions of Ti alloy and (b) -0.5 , -50 , and -500 mA/cm^2 charging cases of bare Ti alloy

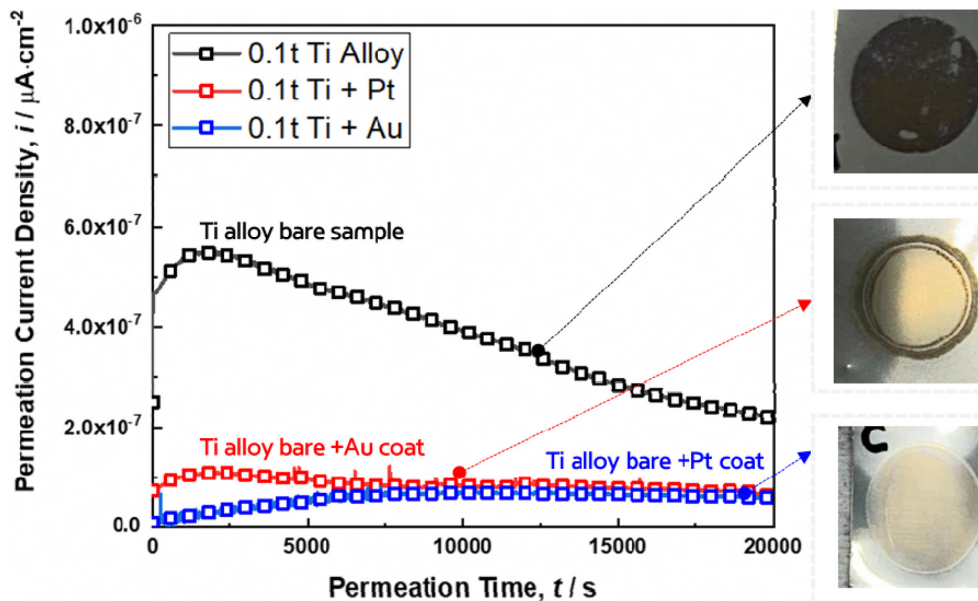


Fig. 5. Hydrogen permeation results on coating conditions of Ti alloy on -500 mA/cm^2

3.3 Effect of noble metal coatings on hydrogen permeation and corrosion – revalidation test

To reconfirm the influence of noble metal coatings (Pt, Au) on Ti alloy under hydrogen charging conditions, an additional set of experiments was conducted focusing on both hydrogen permeation behavior and post-test surface degradation. This revalidation aimed to strengthen the evidence for coating effectiveness in preventing hydrogen ingress and surface corrosion during electrochemical operation.

Fig. 5 shows the permeation current density of bare and coated Ti alloy (0.1t) specimens under a standard hydrogen charging current density of -500 mA/cm^2 . The bare Ti alloy exhibited a peak hydrogen flux of approximately $5.85.0 \times 10^{-7} \mu\text{A}\cdot\text{cm}^{-2}$, which gradually declined over time due to trap site saturation or oxide growth hindering diffusion.

In contrast, the Au- and Pt-coated Ti samples showed significantly reduced permeation. The Au-coated sample displayed a steady-state current of $\sim 1.2 \times 10^{-7} \mu\text{A}\cdot\text{cm}^{-2}$, while the Pt-coated sample exhibited the lowest value, approximately $\sim 8.0 \times 10^{-8} \mu\text{A}\cdot\text{cm}^{-2}$. These values indicate that both coatings effectively suppressed hydrogen transport, with Pt again outperforming Au in this re-test. Visual inspection of the specimen surfaces after permeation testing provided additional confirmation of coating performance:

In case of bare Ti Alloy, severe discoloration and white oxide accumulation were observed, indicating corrosion propagation during hydrogen charging, likely caused by localized acidification and passive film breakdown. In Au-coated Ti, Minor oxide formation was visible, particularly at the edges, suggesting partial coating degradation or pinhole defects allowing localized hydrogen entry and corrosion. Finally, in case of Pt-coated Ti, the surface remained mostly intact with minimal visible corrosion products. This suggests that the Pt coating not only reduced hydrogen permeation but also acted as a robust protective layer against electrolyte-induced surface attack. These findings validate the dual benefit of noble metal coatings—both as hydrogen diffusion barriers and anti-corrosive shields—for titanium-based metallic bipolar plates under PEMFC/PEMWE-relevant environments.

The results from both the initial and revalidation hydrogen permeation tests indicate that the Ti alloy exhibits inherently low hydrogen diffusivity due to its hexagonal close-packed (HCP) crystal structure, which provides limited interstitial paths and a high density of trap sites. However, under sustained charging, the bare Ti alloy still showed a measurable hydrogen flux and significant surface corrosion, confirming that Ti is not fully immune under aggressive electrochemical conditions [11].

Application of noble metal coatings such as Pt and Au

significantly reduced the steady-state hydrogen permeation current density. Among them, the Pt coating exhibited superior performance compared to Au, consistent with its higher density, lower defect tendency during sputtering, and stronger corrosion resistance under acidic conditions [12]. The effectiveness of Pt in reducing both hydrogen ingress and surface degradation can be attributed to its excellent catalytic stability and ability to form uniform, pinhole-free films.

The Au-coated Ti alloy also showed improvement over the bare sample, although localized corrosion was still observed post-test. This could be due to either incomplete coverage or microdefects in the Au layer, which acted as diffusion channels for hydrogen and electrolytes. These results highlight the importance of coating integrity, thickness, and adhesion to ensure long-term performance.

Notably, the visual inspection of the post-test surfaces revealed a strong correlation between permeation current and corrosion severity, supporting the concept that hydrogen ingress exacerbates surface film breakdown and oxide formation. In particular, the bare Ti surface showed clear signs of delamination and whitish corrosion products, while the Pt-coated surface retained its metallic luster with minimal signs of attack.

The findings from this study reinforce the suitability of noble metal coatings for enhancing both hydrogen impermeability and electrochemical durability of metallic bipolar plates. In particular, the Pt-coated Ti alloy emerges as a promising material for PEMFC and PEMWE applications where durability and gas impermeability are critical.

4. Conclusions

This study investigated the hydrogen permeation behavior and corrosion resistance of metallic bipolar plate materials—STS470, STS316L, and a titanium alloy—for applications in PEMFCs and PEMWEs. Emphasis was placed on evaluating the effectiveness of noble metal coatings (Pt, Au) in reducing hydrogen ingress and surface degradation. Electrochemical permeation tests using the Devanathan–Stachurski method were conducted under both standard and high hydrogen charging conditions. Results showed that STS470 had the highest hydrogen permeability among the uncoated materials, while the Ti

alloy and STS316L exhibited minimal permeation. When Pt or Au coatings were applied, the hydrogen permeation current density was significantly reduced across all substrates, with Pt coating showing superior performance. Post-test surface observations confirmed that coated specimens experienced far less corrosion, especially under high hydrogen flux conditions. These findings suggest that noble metal coatings offer a dual benefit of suppressing hydrogen uptake and enhancing electrochemical durability in harsh PEM environments. This study provides several important conclusions for the design and optimization of metallic bipolar plates in PEMFC and PEMWE systems:

1. STS470 (BCC) exhibited the highest hydrogen permeability due to its open crystal structure and low hydrogen solubility. Ti alloy (HCP) and STS316L (FCC) showed superior resistance to hydrogen ingress, consistent with their known trapping behavior and lattice characteristics.

2. Both Pt and Au coatings significantly reduced hydrogen permeation currents, with Pt consistently performing better due to its higher stability, uniform deposition, and superior surface passivation capabilities.

3. Post-permeation surface analyses confirmed that noble metal coatings also mitigate corrosion under acidic environments. Particularly, Pt-coated Ti alloy exhibited minimal surface degradation, making it a strong candidate for long-term bipolar plate applications.

4. Under aggressive hydrogen charging (-500 mA/cm^2), Ti alloy began to show measurable permeation, allowing for clearer differentiation of coating effects. This underscores the necessity of high-flux testing to evaluate coating performance realistically, especially for PEMWE applications.

5. The integration of noble metal coatings on cost-effective substrates like STS470 can provide a viable route to manufacturing durable, hydrogen-resistant, and corrosion-stable bipolar plates for next-generation fuel cell and water electrolysis systems.

Acknowledgments

This work was supported by This work was supported by the Academic Promotion System Tech University of Korea.

References

1. D. Davies, P. Adcock, M. Turpin, and S. J. Rowen, Bipolar plate materials for solid polymer fuel cells, *Journal of Applied Electrochemistry*, **30**, 101 (2000). Doi: <https://doi.org/10.1023/A:1003831406406>
2. H. Wang, M. A. Sweikart, J. A. Turner, Stainless steel as bipolar plate material for polymer electrolyte membrane fuel cells, *Journal of Power Sources*, **115**, 243 (2003). Doi: [https://doi.org/10.1016/S0378-7753\(03\)00023-5](https://doi.org/10.1016/S0378-7753(03)00023-5)
3. S.-J. Lee, J.-J. Lai, C.-H. Huang, Stainless steel bipolar plates, *Journal of Power Sources*, **145**, 362 (2005). Doi: <https://doi.org/10.1016/j.jpowsour.2005.01.082>
4. H. Wang, J. A. Turner, Ferritic stainless steels as bipolar plate material for polymer electrolyte membrane fuel cells, *Journal of Power Sources*, **128**, 193 (2004). Doi: <https://doi.org/10.1016/j.jpowsour.2003.09.075>
5. R. F. Silva, D. Franchi, A. Leone, L. Pilloni, A. Masci, A. Pozio, Surface conductivity and stability of metallic bipolar plate materials for polymer electrolyte fuel cells, *Electrochimica Acta*, **51**, 3592 (2006). Doi: <https://doi.org/10.1016/j.electacta.2005.10.015>
6. O. Ishigami, T. Kondo, Y. Ogawa, Bipolar Plate for Fuel Cell, *World Patent* WO04/070083 (2004).
7. A. Pozio, R. F. Silva, M. De Francesco, L. Giorgi, Nafion degradation in PEFCs from end plate iron contamination, *Electrochimica Acta*, **48**, 1543 (2003). Doi: [https://doi.org/10.1016/S0013-4686\(03\)00026-4](https://doi.org/10.1016/S0013-4686(03)00026-4)
8. P. L. Hentall, J. B. Lakeman, G. O. Mepsted, P. L. Adcock, J. M. Moore, New materials for polymer electrolyte membrane fuel cell current collectors, *Journal of Power Sources*, **80**, 235 (1999). Doi: [https://doi.org/10.1016/S0378-7753\(98\)00264-X](https://doi.org/10.1016/S0378-7753(98)00264-X)
9. M. Li, S. Luo, C. Zeng, J. Shen, H. Lin, C. Cao, Corrosion behavior of TiN coated type 316 stainless steel in simulated PEMFC environments, *Corrosion Science*, **46**, 1369 (2004). Doi: [https://doi.org/10.1016/S0010-938X\(03\)00187-2](https://doi.org/10.1016/S0010-938X(03)00187-2)
10. H.-J. Kim, H.-Y. Jung, T.-W. Kwon, Y.-D. Chung, Effect of Plastic Deformation on Hydrogen Diffusion Behavior of Martensitic Steel in Hydrogen Absorption Environment, *Materials Transactions*, **60**, 1614 (2019). Doi: <https://doi.org/10.2320/matertrans.M2019042>
11. K. Hirata, S. Iikubo, M. Koyama, K. Tsuzaki, and H. Ohtani, First-Principles Study on Hydrogen Diffusivity in BCC, FCC, and HCP Iron, *Metallurgical and Materials Transactions A*, **49**, 5015 (2018). Doi: <https://doi.org/10.1007/s11661-018-4815-9>
12. M. K1st1, S. Uysal, M. F. Kaya, Development of Pt coated SS316 mesh gas diffusion electrodes for a PEM water electrolyzer anode, *Fuel*, **324**, 124775 (2022). Doi: <https://doi.org/10.1016/j.fuel.2022.124775>